HHS Public Access

Author manuscript

Nat Immunol. Author manuscript; available in PMC 2010 February 01.

Published in final edited form as:

Nat Immunol. 2009 August ; 10(8): 907–917. doi:10.1038/ni.1759.

Phagosomal membrane targeting of Irgm1 via PtdIns(3,4)P_2 and PtdIns(3,4,5)P_3 promotes mycobacterial immunity

Sangeeta Tiwari[1], **Han-Pil Choi**[1], **Takeshi Matsuzawa**[1,3], **Marc Pypaert**[2,4], and **John D. MacMicking**[1]

[1]Section of Microbial Pathogenesis, Boyer Center for Molecular Medicine Yale University School of Medicine, New Haven, CT 06510. U.S.A.

[2]Department of Cell Biology, Center for Cell and Molecular Imaging Yale University School of Medicine, New Haven, CT 06510. U.S.A.

Abstract

Vertebrate immunity to infection enlists a new family of 47 kDa immunity-related GTPases (IRGs). One IRG in particular - Irgm1 - is essential for macrophage host defense against phagosomal pathogens including *Mycobacterium tuberculosis* (*Mtb*). Here we show Irgm1 targets the mycobacterial phagosome (PG) via lipid-mediated interactions with phosphoinositide-3,4-bisphosphate (PtdIns[3,4]P_2) and PtdIns(3,4,5)P_3. An isolated Irgm1 amphipathic helix conferred lipid binding *in vitro* and *in vivo*. Mutations in this region blocked PG recruitment and failed to complement the antimicrobial defect in *Irgm1*$^{-/-}$ macrophages. PtdIns(3,4,5)P_3 removal or class I phosphoinositide-3-OH kinase (PI(3)K) inhibition mimicked this effect in wild-type cells. Irgm1-PI(3)K co-operation further facilitated Irgm1 engaging its fusogenic effectors at the site of infection, thereby ensuring pathogen-directed responses during innate immunity.

Keywords

Interferon-gamma; macrophage; tuberculosis; innate immunity

INTRODUCTION

Many of the world's most successful intracellular pathogens reside within host membrane-bound phagosomes (PGs) that provide nutrient access to the recycling endocytic network and shelter from the secreted immune arsenal of antibody and complement. Virulent

Correspondence: John D. MacMicking, Ph.D BCMM 354E, 295 Congress Avenue Yale University School of Medicine New Haven, CT 06510. U.S.A. john.macmicking@yale.edu.

[3]Current address: Department of Veterinary Public Health, Division of Veterinary Science, Graduate School of Life and Environmental Science, Osaka Prefecture University, 1-1 Gakuen-cho, Naka-ku, Sakai 599-8531, JAPAN

[4]Deceased

Author contributions Experimental design, data analysis and interpretation were undertaken by S.T., T.M., H.P.C., M.P. and J.D.M. Molecular and biochemical analyses (affinity purification, gel filtration, yeast-two hybrid, *in vitro* assays) were performed by S.T., H.P.C. and T.M. Scanning confocal microscopy was performed by S.T., T.M., H.P.C and J.D.M. scIEM was conducted by M.P. and J.D.M. The manuscript was written by J.D.M. All authors discussed the results and commented on the manuscript. There are no competing financial interests.

mycobacteria such *M. tuberculosis (Mtb)*, *M. bovis* and *M. avium* are classical examples of persistent micro-organisms that in resting macrophages prevent fusion of their PG niche with lysosomes and autophagolysosomes as a strategy for intracellular survival 1,2. To combat this strategy, vertebrates have evolved innate immune defense mechanisms that facilitate delivery of internalized mycobacteria to acidified secondary lysosomes and intermediates of the autophagic pathway for microbial killing 3-6. How such delivery occurs remains poorly understood but it can be initiated by host cell activation with the T helper type 1 (T_H1) cytokine interferon-γ (IFN-γ), or via Toll-like receptor-4 (TLR4) signaling though the adaptor TRIF 3-6.

The IFN-γ- and lipopolysaccharide (LPS)-responsive GTPase, Irgm1 (also called LRG-47), promotes maturation and acidification of mycobacterial PGs as part of the microbicidal response of *Mtb*-infected macrophages 3-5. The importance of Irgm1 for control of tuberculosis (TB) is evident in both *Irgm1*$^{-/-}$ macrophages and *Irgm1*$^{-/-}$ mice, with the latter proving profoundly susceptible to *Mtb* administered by the natural aerogenic route 3,7. Loss of Irgm1 in macrophages yielded specific defects in PG trafficking along the endolysosomal pathway and did not affect other IFN-γ-induced macrophage effector mechanisms such as those involving nitric oxide synthase 2 (Nos2/iNos), phagocyte oxidase (phox) and Slc11a/Nramp1 (natural resistance associated macrophage protein-1) 3,8-10. Subsequent studies confirmed that Irgm1 and its human ortholog, IRGM, facilitates cell-autonomous resistance to mycobacteria in response to IFN-γ stimulation, TLR4 engagement or cell starvation in murine macrophages and human mononuclear cells 4-6.

Irgm1 belongs to a unique class of IFN-γ-inducible 47-48kDa GTPases (p47 IRGs) - comprising 18-23 genes in mice11,12 - that confer innate immunity to compartmentalized intracellular pathogens13,14. These compartments include bacterial PGs, apicomplexan parasitophorous vacuoles and chamydial inclusion bodies. An emerging paradigm therefore posits the IRGs exerting some of their antimicrobial effects by remodeling the pathogen-containing niche or directing vesicular membrane traffic to and from that compartment 12-14. To date, Irgm1 exhibits the most broadly potent resistance profile of all IRGs tested, being obligate for innate defense against mycobacteria, salmonella, listeria, chlamydia, leishmania, toxoplasma and trypanosomes 12-14. Surprisingly, however, little is known about the molecular basis of how IFN-γ-inducible Irgm1 engages these vacuolar pathogens within infected cells.

Here, we found that Irgm1 uses selective protein-lipid interactions on the nascent PG membrane to co-ordinate its activity for immunity to mycobacterial infection. A protein-gel overlay screen across 33 lipid species uncovered 3 moieties bound by Irgm1: PtdIns[3,4]P_2, PtdIns(3,4,5)P_3 and diphosphatidylglycerol (cardiolipin). *In silico* modeling retrieved a C-terminal lipid binding site that conferred pathogen vacuole attachment; mutations in this region ablated Irgm1 targeting and diminished phagolysosomal fusion. Removal of PtdIns(3,4,5)P_3 on the PG membrane or inhibition of endogenous class I PI(3)Ks and SH2 (Src homology 2)-containing inositol phosphatase-1 (SHIP1; Inpp5d), which are the enzymes responsible for lipid synthesis, also inhibited Irgm1 recruitment to PGs. Irgm1 associated with distinct class I PI(3)K isoforms and enhanced lipid kinase activity; this heightened PI(3)K activity in turn accelerated Irgm1 GTP hydrolysis to promote Irgm1

binding to its fusogenic soluble *N*-ethylmaleimidesensitive factor (NSF) attachment protein [SNAP] receptor (SNARE) effectors at the site of infection. Thus Irgm1 and class I PI(3)Ks comprise a novel signaling platform for orchestrating early PG events needed for subsequent phagolysosomal transfer. These findings yield the first insight into how p47 IRGs are deployed through direct membrane lipid interactions to combat vacuolar pathogens12-14.

RESULTS

Irgm1 trafficking to PG membranes

Irgm1 residence and its trafficking dynamics upon mycobacterial infection were initially characterized via live or fixed cell imaging together with transmission electron microscopy (EM) of immuno-labeled cryosections to delineate membrane structures. Native Irgm1 resided on *cis-medial* (GM130) and small < 50nm post-Golgi vesicles lacking early endosomal autoantigen-1 (EEA-1) in IFN-γ-activated primary mouse bone-marrow derived (BMMs) and RAW264.7 macrophages (Fig. 1a-c). Identical localization was seen in unactivated cells expressing Irgm1 variants tagged with C- or N-terminal enhanced green (EGFP-), yellow (EYFP-), cyan (CFP-) or red fluorescent proteins (RFP-) or tetracysteine (for examples, see Supplementary Fig. 1 online). Endogenous Irgm1 resided on the cytosolic face of Golgi cisternae like other abluminal proteins that also lack a C-terminal Yxx□ motif 15 needed for internal residence (Supplementary Fig. 2 online).

Subsequent infection of IFN-γ-activated macrophages with *M. tuberculosis* variant *bovis* BCG led to rapid Irgm1 relocation from the Golgi to mycobacterial PG (MPG) (Fig. 1b). Endogenous Irgm1 often journeyed great distances - up to 15-30μm - along extended pseudopods to the nascent phagocytic cup enveloping *M. bovis* BCG (Fig. 1b). Irgm1 targeting was observed irrespective of whether mycobacteria expressed EGFP, were Cy5-labeled, or were stained via pan-*Mtb* complex antibody (Ab) or TO-PRO-3 bacterial DNA (Fig. 1b-d). Likewise, fluorescently-tagged Irgm1 variants co-localized regardless of how mycobacteria were detected (Fig. 1d). Both bi-directional controls ruled out nonspecific Ab cross-reactivity and validated the reagents used in this study.

Within 3 h of infection, ~20% of MPGs had recruited Irgm1 and this approached 45% after 6 h, by which stage the pathogen vacuole was often completely coated with the GTPase (Fig. 1c; see inset). After 12 h post-infection (p.i.), ~60% of MPGs were Irgm1$^+$ (Fig. 1c). Time-dependent MPG targeting in part reflects accumulated uptake since phagocytosis of *M. bovis* BCG is asynchronous unless first pre-bound at 4°C-16°C to prevent internalization 3. Under the latter circumstances, MPGs became Irgm1$^+$ much earlier (eg. 60-80% within 6 h; data not shown). Live imaging confirmed that Irgm1 could in fact rapidly translocate to sites of mycobacterial uptake viewed every 8 sec over a 20-frame period (Fig. 1d; see Supplementary Information, Movie 1). Translocation appeared specific, as it occurred at sites of *M. bovis* BCG internalization and not randomly to pseudopod extensions or beneath the plasmalemma elsewhere in the cell. Irgm1 remained PG-associated for at least 6 h p.i. during fusion with (auto)lysosomes visualized with 15nm BSA-gold preloaded during an overnight chase3 (Fig. 1e). Thus Irgm1 partitions between organellar membranes in both uninfected and infected macrophages, residing on Golgi cisternae before prompt deployment to sites of bacterial engulfment 16.

Irgm1 binds PtdIns(3,4)P_2, PtdIns(3,4,5)P_3 and diphosphatidylglycerol

Biochemical fractionation of IFN-γ-activated macrophages substantiated the conclusion that endogenous Irgm1 was largely membrane-associated; ~89% of Irgm1 was present in the detergent-soluble, non-nuclear pellet (Fig. 2a). Other p47 IRG family members including Irgm2 (GTPI; 72%), Irgm3 (IGTP; 88%), Irga6 (IIGP1; 83%) were also membrane-bound, although to a lesser extent than Irgm1 (Fig. 2a).

To identify what membrane lipids Irgm1 interacts with, we screened 33 bioactive species via protein-gel overlay using catalytically-active recombinant Irgm1 fused to glutathione *S*-transferase (rGST-Irgm1). Three moieties strongly interacted with Irgm1: PtdIns(3,4)P_2, PtdIns(3,4,5)P_3 and diphosphatidylglycerol (3-*bis*-*sn*(3'-phosphatidyl)-*sn*-glycerol; cardiolipin) (Fig. 2b). A fourth lipid, phosphatic acid, weakly associated with rGST-Irgm1. Of the remaining p47 IRGs screened, only rGST-Irgm3 displayed conspicuous lipid binding activity that was again weaker than rGST-Irgm1 (Fig. 2b). GST alone or rGST-Irgm1 pre-incubated with 15-fold molar excess (1.5nmol) of each lipid substrate was not detected, confirming the specificity of the interaction (Fig. 2c). Dose-dependent rGST-Irgm1 binding of PtdIns(3,4)P_2 and PtdIns(3,4,5)P_3 among 8 different phosphoinositides was also noted over 1.6-100 pmol range (Fig. 2d). That these interactions could occur within the context of a three-dimensional lipid bilayer was seen using PtdIns(3,4)P_2- or PtdIns(3,4,5)P_3-containing liposomes (Fig. 2e).

Irgm1 C-terminal αK helix confers lipid-binding

We next sought to identify the Irgm1 region(s) involved in binding these lipid species. Lack of transmembrane or post-translational lipid-binding motifs led us to consider an *in silico* approach incorporating secondary structure predictions. Here, low-stringency peptidic blast searches were engrafted onto a computed 3D Irgm1 model based on dimeric Irgb6/IIGP1 (PDB code 1TQ2:2), crystallized in the presence of phosphoaminophosphonic acid-guanylate ester17 (Fig. 3a). This analysis identified polybasic, hydrophobic and amphipathic stretches exposed for membrane targeting. A C-terminal amphipathic alpha helix ([αK] Irgm1$_{350\text{-}374,}$ isoelectric point [pI] 9.0) structurally amenable to lipid membrane interactions was enriched in basic (6/25) plus hydrophobic (14/25) residues (Fig. 3a). Three adjacent helices ([αI,αJ] Irgm1$_{330\text{-}349}$, [αL] Irgm1$_{386\text{-}409}$ also contained basic (αI,αJ - 5/20; αL - 3/24) and hydrophobic (αI,αJ - 6/20; αL - 11/24) residues but had isoelectric points well below that of the overall molecule (6.4 and 6.3 versus 8.3). Modeling also showed that the αL domain packs against the αF helix in an antiparallel orientation, making it unlikely to be membrane accessible.

Direct gel overlay and liposome sedimentation assays confirmed the importance of Irgm1 αK region for lipid binding. Here, the 25 amino-acid rGST-Irgm1$_{350\text{-}374}$ helix recapitulated the lipid interaction profile of full-length rGST-Irgm1 in dose-dependent fashion (Fig. 3b,c). Mutations that destroyed amphipathicity (rGST-Irgm1(F362E,R367E): Fig. 3b, 3d) or replaced specific positively-charged and hydrophobic residues with uncharged, non-hydrophobic alanine (rGST-Irgm1(K350,R352,M354A,C356)) abolished lipid binding (Fig. 3b, 3d). The N-terminal G-domain plus αE,αF helices (rGST-GD$_{75\text{-}289}$) did not recapitulate the lipid binding profile of full-length Irgm1, reinforcing that much of the lipid-binding

activity resides further downstream in the C-terminal αK domain (Fig. 3d). Because αK mutants retained GTPase activity, their failure to bind PtdIns(3,4)P_2, PtdIns(3,4,5)P_3 and diphosphatidylglycerol was not due to gross conformational changes caused by mutagenesis (Fig. 3e).

At physiological pH, PtdIns(3,4)P_2, PtdIns(3,4,5)P_3 and diphosphatidylglycerol can carry net negative charges of -2 to -7 from several PO_4^- moieties 18; these likely interact with polycationic side chains (6 arginines, 1 lysine) within the 25 amino acid αK helix of Irgm1. However, mutations interfering with uncharged, hydrophobic amino acids on the amphipathic face (F362E) also compromised lipid interactions. Thus both charge and non-polar properties are needed for *in vitro* binding of Irgm1 to PtdIns[3,4]P_2, PtdIns(3,4,5)P_3 and diphosphatidylglycerol.

To determine whether these mutations affected Irgm1 membrane binding *in vivo*, we introduced N-terminal EGFP-fused Irgm1 variants into resting primate COS1 or HeLa cells devoid of endogenous Irgm1 expression. Like native Irgm1, EGFP-Irgm1 localized to the *cis*-Golgi with the αK fragment sufficient to direct organelle targeting (EGFP-α$K_{350-374}$; Fig. 3f) 16. Membrane targeting of the lipid-binding mutants EGFP-Irgm1(F362E,R367E) and EGFP-αK (F362E,R367E), however, was completely lost (Fig. 3f). Fragments encompassing adjacent amphipathic αI,J (EGFP-Irgm1$_{330-349}$; Fig. 3f), αE,F (EGFP-αE,$F_{254-289}$), αG,H (EGFP-αG,$H_{290-327}$) and αL helices (EGFP-α$L_{375-409}$) also failed to target the Golgi membrane (data not shown) 16, confirming earlier *in silico* predictions that these regions lacked the requisite characteristics for lipid binding. Of the lipid moieties bound *in vitro* by Irgm1, only diphosphatidylglycerol was conspicuously present on Golgi cisternae (Supplementary Fig. 3 online). Strong PtdIns(3,4)P_2 and PtdIns(3,4,5)P_3 staining was absent from Golgi stacks; thus the role of these lipids may instead be to target Irgm1 to the PG membrane during infection.

Irgm1 targeting to MPGs promotes immunity

First we determined if PtdIns(3,4)P_2 and PtdIns(3,4,5)P_3 are generated at sites where Irgm1 accumulates. EYFP fused to the pleckstrin homology domains (PH) of tandem-PH domain containing protein-1 (EYFP-PH-TAPP1; 80nM K_d for PtdIns(3,4)P_2)19 or of general receptor for phosphoinosides protein-1 (EYFP-PH-GRP1; 170nM K_d for PtdIns(3,4,5)$_3$)19 were nucleoporated into IFN-γ-activated macrophages that were subsequently infected with Cy5-labelled *M. bovis* BCG. Live imaging often revealed bursts of PI(3,4,5)P_3 synthesis that coincided with rapid recruitment (~10-20 s later) of CFP-Irgm1 to sites of bacterial internalization (Fig. 4a). CFP-Irgm1 was also recruited to PtdIns(3,4)P_2-enriched phagocytic cups but here the appearance was transient and occurred at slightly later times (2-5 minutes p.i., Supplementary Fig. 4 online).

Thus a switch from PM-derived PtdIns(3,4,5)P_3 to PG-derived PtdIns(3,4)P_2 may accompany vacuole maturation, eventually leading to PI(3)P generation alongside that synthesized *de novo* by the class III PI(3)K Vps34p 20. Indeed, using the PX domain of NADPH phox40 subunit fused to EYFP (EYFP-p40-PX) as a PtdIns(3)P-specific sensor 20, *M. bovis* PGs became positive for this probe ~5-15 minutes after Irgm1 was recruited (Supplementary Fig. 4 online). Diphosphatidylglycerol (cardiolipin) was also detected on

MPGs at later times (~10-30 min p.i. Supplementary Fig. 4 online) but, unlike PtdIns(3)P, its presence partly depended on bacterial viability (data not shown). *Mtb* secretes lysocardiolipin that is exported from PGs following cleavage by host lysosomal phospholipase A2 21; thus some PG lipid detected via anti-cardiolipin is probably pathogen- rather than host-derived. Delayed appearance of diphosphatidylglycerol on PG membranes also suggests that the main function of this lipid may be to help retain, rather than recruit, Irgm1.

What regions of Irgm1 are needed for its recruitment to MPGs? EGFP-αK but not the neighboring EGFP-αI,αJ region was sufficient to target MPGs (Fig. 4b,c). Some 30% of PGs became αK-positive within 3-12 min of bacterial uptake. Recruitment was lost, however, when PtdIns-binding mutations were introduced into the αK helix (EGFP-αK(F362E,R367E)) or full-length protein (EGFP-Irgm1(F362E,R367E)) or when the C-terminus containing αK was removed (EGFP-$GD_{75\text{-}292}$)(Fig. 4b,c). Importantly, nucleoporation of EGFP-Irgm1 but not EGFP-Irgm1(F362E,R367E) into primary IFN-γ-activated *Irgm1*$^{-/-}$ BMMs rescued MPG transfer to proteolytically-active lysosomes as measured by dequenching of difluoro-4-bora-3α,4α-diaza-*s*-indacene conjugated to bovine serum albumin (DQ Red BSA) (Fig. 4d; Supplementary Fig. 5 online). Thus an intact αK domain is necessary and largely sufficient to target Irgm1 via lipid-protein interactions to MPGs where it functions to promote antimicrobial activity.

Class I PI(3)K and SHIP1-derived PtdIns help recruit Irgm1

Irgm1 employs the same domain for PG targeting *in vivo* that is used for PtdIns binding *in vitro*. Moreover, PtdIns(3,4)P_2 and PtdIns(3,4,5)P_3 are both present at sites where Irgm1 engages the PG membrane. Are these lipids responsible for MPG recruitment of Irgm1? We addressed this question by depleting local PtdIns(3,4,5)P_3 or removing the enzymatic source of these lipid species - class I PI(3)K isoforms and the type II phosphatase, SHIP1 - *in vivo*. Class I PI(3)Ks generate both PtdIns(3,4)P_2 and PtdIns(3,4,5)P_3; SHIP1 dephosphorylates Ins(1,3,4,5)P_4 and PtdIns(3,4,5)P_3 to yield PtdIns(3,4)P_2. These mammalian enzymes are the primary sources of PtdIns(3,4)P_2 and PtdIns(3,4,5)P_3 in haematopoietic cells 22 such as macrophages and have recently been found on artificial (eg. latex bead) or erythrocyte PGs 23,24.

First, local PtdIns(3,4,5)P_3 was removed by targeting a yeast PtdIns(5)P-specific phosphatase, Inp54p 25, to MPGs. Here, Inp54p was fused to FKB that upon rapamycin (Rap) treatment dimerizes with FKBP already tethered to PGs via a Lyn kinase PM motif. This strategy enabled Inp54p to deplete PtdIns(4,5)P_2 and PtdIns(3,4,5)P_3 specifically on early PG membranes, ruling out potential interference with these lipids in Irgm1 exit from the Golgi. Simultaneous PI(3)K inhibition by wortmannin was also used to ensure any residual PtdIns(4,5)P_2 is not converted to PtdIns(3,4,5)P_3. CFP-Inp54p-FRB bound FKBP on MPG membranes within 4-12 minutes of Rap exposure (Fig. 5a). Dimerized CFP-Inp54p-FRB markedly inhibited Irgm1 trafficking to the MPG by 55.4% in the absence of wortmannin, confirming that the site of PtdIns(3,4,5)P_3 synthesis is a important spatial cue directing Irgm1 recruitment (Fig. 5a). Neither Rap alone nor Inp54p minus Rap affected Irgm1 translocation (Fig. 5a). Wortmannin alone inhibited translocation by 67.2%, as scored

by “inside-out” staining to mitigate any effects on mycobacterial uptake 26 (see Supplementary Fig. 6 online). Thus other 3'-phosphate-containing lipid species such as PtdIns(3,4)P_2 are needed along with PtdIns(3,4,5)P_3 to recruit Irgm1 to MPGs (Fig. 5a). That both lipids are important is underscored by the observation that combined Rap-Inp54p plus wortmannin treatment was the most effective intervention (75.4% inhibition; Fig. 5a).

Next, we determined which class I PI(3)K isoforms generate the Irgm1-binding lipids needed for MPG recruitment. This question became relevant since wortmannin affects all PI(3)K classes (IC_{50} ~3-5nM) as well as mTOR, DNA-PK, ATM and class II PIPkins α and β 22,27. We probed the requirement for ~110kDa catalytic (Class IA: Pik3ca, Pik3cb, Pik3cd; Class IB: Pik3cg) and 85kDa regulatory (Pik3r1-r2) subunits through isoform-specific drug inhibition or siRNA treatment; we also used siRNAs to silence SHIP1 (Fig. 5b). A thieno[3,2-*d*]pyrimidine derivative 15e was used to block Pik3ca (IC_{50}, ~2nM) 28, TGX-221 to block Pik3cb and Pik3cd (IC_{50}, ~50-500nM at cytosolic 1mM ATP) 29,30 and AS-252424 to block Pik3cg (IC_{50}, 35nM) 30. Only 15e proved singly effective in inhibiting Irgm1 relocation (39.1%) whereas all three drugs together exerted a more pronounced effect than 15e alone (56.3% inhibition; Fig. 5c,d). Their action appeared specific for class I PI(3)K activity; PtdIns(3)P-binding EEA-1 was still recruited to MPGs 20, indicating class III PI(3)K PtdIns(3)P 26 generation was intact (Supplementary Fig. 7 online). siRNA treatment showed that both Pik3r1-r2 85kDa subunits (and possibly their 55kDa splice variants 22, Fig. 5b) along with SHIP1 were also needed for Irgm1 relocation (48.2-62.9% inhibition; Fig. 5c,d). Thus Pik3ca-Pik3r1-r2 heterodimers appear to be the major class I PI(3)K isoforms acting with SHIP1 to furnish PtdIns(3,4)P_2 and PtdIns(3,4,5)P_3 at sites of Irgm1 targeting on the nascent PG membrane.

Interplay between Irgm1 and class I PI(3)K

Scanning meta-confocal microscopy found Irgm1, Pik3ca, Pik3r1-r2 and SHIP1 together on phagocytic cups engulfing mycobacteria (Fig. 5e). Moreover, Irgm1 physically interacted with Pik3ca and with both Pik3r1and Pik3r2 subunits, strengthening the idea that PtdIns synthesis and Irgm1 recruitment are spatially linked. Flag-Pik3ca bound EGFP-Irgm1 (Fig. 6a) as well as known Pik3ca interactors, HA-$p21^{Ras}$ and its constitutively-active variant, HA-$p21^{RasQ61L}$ (data not shown) 31. Flag-Pik3ca did not, however, co-immunoprecipitate EGFP alone(Fig. 6a), EGFP-Pik3cb, EGFP-Pik3cg, or SHIP1, nor was it captured by an irrelevant isotype-matched IgG (data not shown). Likewise, Myc-Irgm1 bound EGFP-Pik3r1 and EGFP-Pik3r2, albeit consistently weaker than EGFP-Pikca (Fig. 6b). A similar outcome was seen in direct GST pulldown assays (Fig. 6c,d). Irgm1-Pik3ca interactions relied on regions outside of the αK helical region; EGFP-Irgm1, EGFP-Irgm1(F362E,R367E) and EGFP-$GD_{75\text{-}292}$ all bound Flag-Pik3ca whereas EGFP-αK did not (Fig. 6e). Thus lipid- and PI(3)K-binding interfaces of Irgm1 appear to be distinct.

What are the biochemical consequences of Irgm1-PI(3)K interactions? rGST-Irgm1 accelerated Pik3ca-Pik3r1 heterodimer-mediated PtdIns(4,5)P_2 phosphorylation to PtdIns(3,4,5)P_2 (Fig. 6f). This effect was blocked by wortmannin (Fig. 6f). Two positive controls, HA-$p21^{Ras}$ and HA-$p21^{RasQ61L}$, as well as the GTPase-inactive rGST-Irgm1(S90N) mutant also accelerated PtdIns(4,5)P_2 phosphorylation (Fig. 6f). Thus Irgm1

functions like $p21^{Ras}$ to enhance lipid kinase activity although, unlike the latter 31, it does not strictly rely on nucleotide catalysis or G-domain conformation.

PI(3)K likewise regulated Irgm1 catalysis. rPik3r1 increased Irgm1 GTPase activity in single-turnover GAP assays; this effect was abolished by Arg274 mutations within the Pik3r1 Ras binding domain (RBD; rPik3r1(R274A)), a region known to serve as a Rab5GAP 32 (Fig. 6g). Highly-purified rPik3r1 induced more modest increases in Irgm1 GTPase activity compared with Rab5 (400nM rPik3r1 used per reaction due to limited supply versus 10μM described previously33) (Fig. 6g). Nonetheless, enhanced activity was still evident.

We also found that PtdIns(3,4)P_2 and PtdIns(3,4,5)P_3-dependent lipid-binding enhanced Irgm1 catalysis. In these experiments we directly measured GTPase activity of Irgm1 on liposomes incorporating either 5% mol/mol PtdIns(3,4)P_2 or PtdIns(3,4,5)P_3 (Fig. 6h). Lipidtethered rGST-Irgm1 but not rGST-Irgm1(F362E,R367E) exhibited marked increases in catalysis (2.82-3.62 fold) versus liposome-free (Fig. 3e) or control PC:PE liposome samples (Fig. 6h,i). In structural terms, intramolecular inhibition exerted by the αK helix may be relieved after binding lipid bilayers 33; this effect could account for the increased GTPase activity of liposome-bound Irgm1. Likewise, Irgm1(F362E,R367E) exhibited heightened activity versus Irgm1 in the absence of lipid (7.15 ± 0.83 v. 1.42 ± 0.20 nmol GTP hydrolyzed/min/nmol protein) (Fig. 6h,i), suggesting it may already adopt a conformation analogous to lipid binding. Thus specific PtdIns not only provide spatial cues for MPG recruitment but can act as an allosteric switch 33 for Irgm1 catalysis once the latter is targeted to this environment.

Irgm1-PI(3)K co-operation engages fusogenic effectors

How do enhanced Irgm1 and class I PI(3)K catalytic activities benefit anti-mycobacterial immunity? Accelerated GTP hydrolysis may promote binding of Irgm1 to fusogenic partners that induce MPG maturation. Alternatively, elevated class I PI(3)K synthesis of PtdIns(3,4,5)P_3 and resultant PtdIns(3,4)P formation could help bring Irgm1 effectors in close proximity with the GTPase. Either outcome would reinforce the other.

To test the first possibility, we conducted a yeast-2 hybrid (Y2H) screen to isolate fusogenic partners, as Irgm1 effectors have not been identified. Two membrane trafficking proteins - Snapin (soluble *N*-ethylmaleimide-sensitive factor (NSF) attachment protein [SNAP]-associated protein) and Tmed10 (transmembrane emp24-like trafficking protein 10) - were retrieved in this screen (Fig. 7a). Snapin binds to t-SNARE complex proteins on donor membranes and promotes accelerated fusion with cognate v-SNARE-expressing compartments (eg. lysosomes) 34-36. Tmed10, in contrast, assists COPI and COPII transport between the Golgi and ER39. As such we focused on Snapin given its fusogenic function and importance for mycobacterial control (H.P.C, S.T., T.M., J.D.M., manuscript in preparation).

Snapin bound to Irgm1 and a known t-SNARE interactor, Snap23 34, in coimmunoprecipitation (Fig. 7b) and GST pulldown (Fig. 7c) assays. Snapin binding was blocked using a non-hydrolyzable Irgm1 substrate, GTP-γ-S, and was increased using GDP

plus aluminum fluoride (AlF_x) that allows Irgm1 to adopt the transition state conformer, mimicking structural changes during hydrolysis 33 (Fig. 7C). Thus heightened GTPase activity brought about by Pik3ca-Pik3r1, PtdIns(3,4,5)P_3 and PtdIns(3,4)P_2 may favor Irgm1 binding its fusogenic effectors. Likewise, protein-gel overlay showed that Snapin specifically interacted with PtdIns(3,4,5)P_3, PtdIns(3,4)P_2, PtdIns(3)P and to a lesser extent, PtdIns(4)P (Fig. 7d). Thus elevated lipid kinase activity could help retain Irgm1 effectors like Snapin on the PG.

Both possibilities were tested by chemical and genetic loss-of-function approaches. First, co-immunoprecipitation of Irgm1 by Snapin was conducted in the presence of 15e, TXG-221, and AS-252424. Inhibition of class I PI(3)K activity severely reduced Irgm1-Snapin interaction (Fig. 7e). Second, PtdIns-binding mutations greatly diminished the ability of Irgm1 to bind Snapin in untreated cells (Fig. 7f). Thus lipid-mediated targeting of Irgm1 is critical for this GTPase to engage its effectors, most likely at the site of infection since endogenous Snapin strongly localized to PGs in *M. bovis*-infected macrophages (Fig. 7g). Notably, Snapin targeting itself did not require lipid kinase or Irgm1 activity; it still localized to MPGs in primary IFN-γ-activated *Irgm1*$^{+/+}$ and *Irgm1*$^{-/-}$ macrophages treated with 15e, TXG-221 and AS-252424 (Fig. 7g; Supplementary Fig. 8 online). Class I PI(3)K products therefore aid recruitment of the GTPase rather than sequestration of the effector. Such a model is consistent with the weak coimmunoprecipitation of Snapin by Irgm1(F362E,R367E) because the latter cannot translocate to PG membranes (Fig. 4b,c). PI(3)K-mediated MPG targeting of Irgm1 thus promotes access of the GTPase to its fusogenic partners for facilitating SNARE complex assembly. In summary, these findings indicate that PI(3)K-derived PtdIns help integrate recognition and effector events that confer Irgm1-mediated defense against phagosomal pathogens.

DISCUSSION

Here we identified PtdIns(3,4)P_2 and PtdIns(3,4,5)P_3 as important spatial cues for Irgm1 recognition of nascent PG membranes within minutes of bacterial uptake. Once recruited, Irgm1 co-operates with resident class I PI(3)Ks for binding effectors to initiate its antimicrobial activity.

These findings parallel a recent landmark study of the Ras, Rab, Arf and Rho GTPases wherein nearly a third of 125 proteins examined were peripherally targeted via PtdIns(4,5)P_2 and/or PtdIns(3,4,5)P_3 in uninfected fibroblasts 25. As basal concentrations of PtdIns(3,4,5)P_3 are typically low (5μM), either high-affinity PH domains (30-40mM range) or steep PtdIns(3,4,5)P_3 increases following cellular activation are needed for lipid selectivity 26,39. The latter occurs after IFN-γ treatment, which activates class IA PI(3)Ks and PDK via PKCδ 40. Moreover, mycobacterial infection can lead to PtdIns(3,4)P_2 generation at the phagocytic cup through 5' dephosphorylation of PtdIns(3,4,5)P_3 by SHIP1 24,25. Inhibition of these enzymes pharmacologically or genetically, or removal of their localized products, interfered with Irgm1 translocation to this compartment. Notably, such interference was robust but incomplete (48.2-75.4% inhibition), as was αK helix localization to PtdIns(3,4)P_2- and PtdIns(3,4,5)P_3-positive MPGs. Thus additional factors contribute to membrane recruitment, including Pik3ca that binds Irgm1 outside of its polybasic αK region

and Snapin which may help retain Irgm1 on the PG surface. Indeed, the presence of protein anchors could account in part for the persistence of Irgm1 on MPGs at a time when the anionic charge on the inner PM leaflet should have long since dissipated 40.

Besides acting as a temporospatial cue, PtdIns(3,4)P_2 and PtdIns(3,4,5)P_3 binding may also function as an allosteric switch. Increases in GTPase activity for wild-type Irgm1 after liposome binding, or of Irgm1(F362E,R367E) during lipid-free assays, support the idea that conformational changes within the αK region de-repress a molecular inhibition often seen in PH-like domains 33,38. Both the PH β-sheet orthogonal sandwich 41 and αK amphipathic helix share strong charge polarity with one edge of the curved sheet or helix being much more positive than the other. This enables direct interactions with the PO_4^{2-} lipid head group to elicit conformational changes that either remove steric hindrance of an active site or promote self-assembly 17,33,41.

In addition, Irgm1 GTPase activity could be accelerated via an accessory GAP. Incubation of Irgm1 with Pik3cr1 (p85α) led to elevated ^{32}P-γ-GTP hydrolysis via the latter protein's RBD. This domain exerts a similar effect on active GTP-bound Rho family members Cdc42 and Rac as well as endosomal Rab5 32,41. Point mutations at Pik3r1 R274A destroy Rab5 GAP function; here this point mutation also abolished increases in Irgm1 GTPase activity. In the case of Rab5, binding to Pik3ca-Pik3r1 stimulates *in vitro* homotypic endosome-endosome fusion 42. Irgm1 GTPase activity is likely to instead facilitate fusion between MPGs and endo- or autolysosomes 3,5,36.

Supporting this conclusion, GTPase-deficient Irgm1(S90N) fails to complement the fusogenic defect in *Irgm1*$^{-/-}$ macrophages (H.P.C, S.T., T.M., J.D.M., manuscript in preparation); this failure is in part due to the fact that GTPase activity is required to assemble SNARE adaptors that preferentially bind the Irgm1 transition-state conformer. Thus Pik3ca-Pik3r1 may help hydrolyze newly-recruited Irgm1 which, in its transition-state, captures fusogenic partners. Such an exchange likely takes place on phagocytic cups since both enzymes localize to these regions and class I PI(3)K inhibitors interfere with Irgm1-Snapin binding. Moreover, GTP hydrolysis only appears effective after Irgm1 is first recruited to Snapin-positive MPGs, as Irgm1(F362E,R367E) failed to rescue the lysosomal targeting defect in IFN-γ-treated *Irgm1*$^{-/-}$ macrophages despite its elevated catalytic activity. Once recruited, Irgm1 probably regulates effectors for the next stage of phagolysosomal transfer in what is largely a Pik3ca-Pik3r1/2-independent manner. This is because PtdIns(3,4,5)P_3 and PtdIns(3,4)P_2 are metabolized soon after PG closure 23,38,40. Such a proposal fits with earlier observations that Pik3r1-r2$^{-/-}$ murine embryonic fibroblasts have major deficiencies in PG formation but not maturation 26.

Based on our results, a model emerges in which translocation events could be considered “activating” by helping to bring a structurally-favored Irgm1 in close proximity with binding partners such as GAPs or SNARE components that mediate subsequent fusogenic activity. Indeed, IFN-γ-induced phagolysosomal transfer is essential for mycobacterial killing; genetic lesions that block lysosome delivery (*Irgm1*$^{-/-}$, *Atg5*$^{-/-}$) 3,44 or accelerate it (*coronin-1*$^{-/-}$) 45 inhibit or promote macrophage tuberculocidal activity, respectively. So, too, do drugs that either prevent PG acidification (Bafilomycin A, omeprazole) 3 or relieve

PG maturational arrest (H-89, which targets AKT1) 46. Both lines of evidence underscore the importance of non-oxidant defense against mycobacteria and the contribution of IFN-γ-induced Irgm1 to that process. In addition, recent evidence implicates Irgm1 in autophagic regulation of $CD4^+$ lymphocyte survival 47, suggesting this GTPase utilizes common organizing principles to exert specialized membrane regulatory functions during innate as well as acquired immunity. Such widespread cellular involvement may explain why Irgm1 deficiency results in susceptibility to so many diverse phagosomal pathogens 3,7,12-14. Our studies provide the first molecular glimpse of how Irgm1 uses lipid-protein interactions to initiate its antimicrobial activities against a classic membrane-bound organism.

METHODS

Nucleoporated plasmids

We used 16 Irgm1 and 7 class I PI(3)K plasmids: EGFP-Irgm1, Irgm1-EGFP, EYFP-Irgm1, CFP-Irgm1, RFP-Irgm1, EGFP-Irgm1(F362E,R367E), EGFP-GD_{75}-289, EGFP-αE,$F_{254-289}$, EGFP-αG,$H_{290-327}$, EGFP-αI,$J_{328-349}$, EGFP-α$K_{350-374}$, EGFP-αK(F362E,R367E), EGFP-α$L_{374-409}$, Irgm1-C_6, Flag-Irgm1, Myc-Irgm1, EGFP-Pik3ca, EGFPPik3cb, EGFP-Pik3cg, EGFP-Pik3r1, EGFP-Pik3r2, Flag-Pik3ca and YFP-Pik3r1-Flag. HA-tagged $p21^{Ras}$ and HA-$p21^{RasQ61L}$ served as controls. Myc-Snapin and Flag-Snap23 were cloned for effector studies. Point mutations were generated via QuikChange (Invitrogen). A complete list of plasmids and primers is found in Supplementary Table 1 online.

Cell culture, transfection and mycobacterial infection

Primary BMMs from congenically-matched *Irgm1*$^{+/+}$ or *Irgm1*$^{-/-}$ mice maintained under specific-pathogen free conditions (SPF) were differentiated as described 3. All mice were handled according to institutional guidelines for animal care and use. RAW264.7, COS-1, HeLa and HEK cells (ATCC) were cultured in either RPMI or DMEM (containing 10% heat-inactivated FBS, 4mM L-glutamine, 100 U/ml penicillin G, 100μg/ml streptomycin). Cells were nucleoporated (Amaxa) to avoid lipid carrier-based transfection reagents that might interfere with protein trafficking, or viral-mediated gene delivery that might activate control cells. Recombinant mouse IFN-γ (R &D; 100U.ml^{-1}) was added 4 h post-nucleoporation and *M. bovis BCG* (MOI, 5:1) 20h later for a 60 min chase period. *M. bovis* BCG (Phipps strain) or recombinant BCG (Pasteur) harboring an episomal GFP(S65T) bright mutant (rBGP-GFP) 48 were grown in 7H9 broth (GIBCO) plus 10% OADC; the latter strain was kept under 25μg/ml kanamycin selection. Cy5-labelling of BCG was conducted in 0.1M $NaCHO_3$ buffer, pH 9.3, followed by amino group neutralization and washing with 50mM Tris buffer, pH 8.0. Heat-killed bacteria was confirmed by 7H10 agar plating.

Antibodies

All were rabbit, goat or donkey primary Abs unless otherwise stated: Anti-Irgm1 (A19), anti-Irgm2 (M14), anti-Irgb6 (G20), anti-Pik3r1 (Z8), anti-Pik3r2 (T15) and anti-Inpp5d (P1C1) were from Santa Cruz Biotechnology; anti-Pik3ca (4255), anti-Pik3cg (4252), anti-Pik3r1/r2 (4292) were from Cell Signaling; anti-Irgm3 (7) and anti-Pik3ca (19) were from BD Biosciences; anti-actin (A2066), anti-GST mAb (G1160) and anti-FLAG M2 (F3165)

were from Sigma. We also used anti-Pik3ca (AP8016, Abgent), anti-EEA-1 (324610, Calbiochem), anti-cardiolipin (human IgG HCL-0100, Immunovision), anti-*Mtb* complex (B65601B, Biodesign International), anti-Snapin (148002, Synaptic systems); anti-HA (MMS-101R, Covance), anti-GFP (7.1/13.1, Roche), anti-GM130 (G. Warren, Vienna) 49, donkey anti-goat, anti-mouse, and anti-rabbit Ig-Alexa488 or Alexa594 (A1105, A-21203, A21207) and anti-Myc (9E10) (Molecular Probes-Clontech).

4D confocal and cryo-electron microscopy

For live imaging, 2×10^5 macrophages were nucleoporated, dispensed onto MatTek glass-bottom dishes and activated for 16-24 h with IFN-γ ($100U.ml^{-1}$). rBGP-GFP or Cy5-BCG were pulse-chased for 40-60 min before recording at 37°C under oil (100x objective) on a Zeiss LSM510 confocal microscope in MetaDetector mode. Compressed Z-series were deconvolved using AutoQuant 3D (InVision) or ImageJ (NIH) software to yield 4D data over time. When applied, pseudocoloring used original pinhole, Airy disc and intensity gain settings. Static images were captured on 3% PFA-fixed samples. Cardiolipin was detected via a nonyl acridine orange stain 50. EM cryosections were processed as described 49 and stained with A19 or anti-EGFP followed by either rabbit anti-goat or anti-mouse (Jackson Immunochemicals) and then Protein A-10nm gold. BSA-gold (15nm) tracer was pulse-chased into IFN-γ activated macrophage lysosomes overnight and unsonicated BCG (MOI 10:1) added for 60 min at 16°C. Mycobacterial uptake was initiated by shifting to 37°C to allow phagosomal trafficking for 6 h 3.

Recombinant proteins

GST-tagged proteins were expressed in bacteria (*E. coli* BL21DE3-RIPL), isolated using glutathione Sepharose 4B and desalted using GST- or Sephadex G-25 superfine Hi-Trap (to remove trace $MgCl_2$) via fast protein liquid chromatography (FPLC). These proteins included rGST-Irgm1, rGST-Irgm1(S90N), rGST-Irgm1(F362E,R367E), rGSTIrgm1(K350,R352,M354A,C356A), rGST-α$K_{350-374}$, rGST-GD_{75-292}, rGST-Irgm2, rGST-Irgm3, rGST-Irgb6, rGST-Rab5a, rGST-Pik3r1, rGST-Pik3r1(R274A) rGST-Snapin and rGST alone. Soluble Pik3r1, Pik3r1(R274A) and Snapin were generated via Precision protease cleavage (2U/mg protein). His_6-Snapin (pET-28a, Novagen) was isolated on Ni^{2+} columns and subjected to FPLC as above.

Membrane fractionation, protein-lipid gel overlay and liposome assays

Fractionated lysates (Subcellular Proteome Extraction, Calbiochem) were immunoblotted with anti-Irgm1, anti-Irgm2, anti-Irgm3 or anti-Irgb6 before quantitation via densitometry. For protein-gel overlay, nitrocellulose filters harboring biologically-active lipids (Echelon) were blocked with 0.1% OVA in TBST (10mM Tris pH 8.0, 150mM NaCl, 0.1% Tween-20) before adding molar equivalents of each GST-fusion protein (13.7 nmol) plus anti-GST. After washing, filters were incubated with secondary anti-mouse IgG_{2a} (Jackson Immunochemicals) before detection via ECL Plus kit (Amersham). Liposome binding used 1mM PC:PE:biotin-PE (65%:29%:1% mol:mol) liposomes (Echelon) with 5% PtdIns(3,4,5)P_3 or PtdIns(3,4)P_2 incorporated. GST-fusion proteins were added at 25°C in 50 mM Tris pH 7.5, 150 mM NaCl, 0.05% NP-40 buffer with shaking. Liposome aliquots

were removed for immunoblotting the pre-pellet load before centrifugation (20,000 x *g*, 20 min) and washing cycles. The pellet was then immunoblotted with anti-GST for detection of sedimented rGST-Irgm1 in the post-pellet fraction.

Irgm1 structural modeling

An Irgm1 homology model was generated in Modeller (9v1, 1) using the crystal structure of Iigp1 (Irga6) bound to Mg^{2+} and GNP (phosphoaminophosphonic acid guanylate ester; PDB code 1TQ2; 2) with a manually curated sequence alignment based on Probcons and 3DPSSM. The GROMOS96 force-field in SwissPDB Viewer (v3.7; http://www.expasy.org/spdbv/) was used for energy minimization. Structures were rendered using PyMol (www.pymol.org) 12.

GTPase assays

$\tilde{\gamma}[^{32}P]$GTP hydrolysis by 200nM rGST, rGST-Irgm1, rGST-Irgm1(S90N),rGST-Irgm1(F362E,R367E) in reaction buffer (50mM Pipes (pH 7.0), 5mM $MgCl_2$, 10μM GTP, 100nM $\tilde{\gamma}[^{32}P]$GTP)was assayed at 37°C. After charcoal column removal of GDP and GTP, liberated P_i was measured via scintillation counter. Heat-inactivated GST-Irgm1 served as a negative control. Where used, 500 μM liposomes were pre-incubated with substrate and enzyme for 10 min before addition of $MgCl_2$ to initiate the reaction. Single turnover GAP assays were performed using 200nM rGST-Irgm1 or rGST-Rab5a immobilized on glutathione Sepharose 4B beads for pre-binding 500 nM $\tilde{\gamma}[^{32}P]$GTP. Unbound substrate (>99.7% as measured via scintillation counting) was removed by repeated washing and rPik3r1 or rPik3r1(R274A) (400nM) added to bind Irgm1 and Rab5a (positive control) for 10 min before catalysis. rGSTIrgm1 or rGST-Rab5a without Pik3r1 reactions served as controls. Neither rPik3r1 or rPik3r1(R274A) alone displayed $\tilde{\gamma}[^{32}P]$GTP hydrolyzing activity (data not shown).

MPG and PM PtdIns depletion *in vivo*

Macrophages were nucleoporated with constructs encoding FRB-CFP-Inp54p, Lyn11-FKBP and EYFP-Irgm1, pre-activated with IFN-γ and pulsed for 15 min with 10μM rapamycin in the presence or absence of 500nM wortmannin throughout the assay. Cells synchronously-infected with Cy5-BCG were then live-imaged for 3 h. Z-series identified the percentage of uninternalized bacteria; this percentage closely matched the percentage obtained from non-permeabilized coverslips co-stained with anti-*Mtb* pAb coupled to Alexa488 to detect external Cy5-BCG (“inside-out” staining, Supplementary Fig. 5 online). Autophagy was not observed with 10μM rapamycin for 15 min as this drug induces strong autophagic responses only when present at 50-100μM for longer periods (e.g. 2h) in RAW264.7 macrophages 4,5.

Class I PI(3)K gene silencing and pharmacologic inhibition

siRNAs (siGENOME SMARTpools, Dharmacon) were nucleoporated and 4 h later IFN-γ was added for 16-20 h before infection. siRNAs used were Pik3r1 (L-041079-00-0005), Pik3r2 (L-041085-00-0005), SHIP1 (Sc-36491, Santa Cruz), control (ON-TARGET plus Non-targeting). Gene silencing was confirmed by immunoblot. Chemicals were used at 10-500 fold $>IC_{50}$ concentrations to ensure inhibition but 4-5 fold $< IC_{50}$ of other class I

PI(3)K isoforms to retain selectivity (1μM for 15e, μM for TXG-221 and 350nM for AS-252424) 28-30. Such treatment inhibited Flag-Pik3ca-Pik3r1 or Flag-Pik3cb-Pik3r1 activity in an isoform-specific fashion. Drug uptake was enhanced by incubation in serum-free plus phosphate-free media 20 min before *M. bovis* infection and in complete media thereafter.

Lipid kinase assays

Class I PI(3)K activity was measured via ELISA sandwich assay (K-2600, Echelon) on HEK cells transfected with both heterodimeric subunits, Flag-Pik3ca and Pik3r1-Flag, before capture and washing on 50% Protein G-agarose with TNE (10mM Tris-HCl, pH 7.4, 150 mM NaCl and protease as well as phosphatase inhibitors). PI(3)K reaction buffer supernatants (2.5 mM $MgCl_2$, 5 mM Hepes pH 7, 25 μM ATP) containing 500 pmol $diC_8PtdIns(4,5)P_2$ with or without rGST-Irgm1 variants (1.6μM) were incubated for 3 h at 25°C, after which $PtdIns(3,4,5)P_3$ was measured as per the manufacturer's protocol. Transiently-expressed HA-tagged $p21^{Ras}$ or HA-$p21^{RasQ61L}$ were immunoprecipitated and TEV-cleaved, with the resulting soluble proteins were added to Pik3ca-Pik3r1 as a positive control. Wortmannin (500nM) or 15e (μM) added 20 min prior to the reaction served as negative controls.

Yeast 2-hybrid screen

Screening was performed using MATCHMAKER GAL4-based twohybrid system III (BD Biosciences, Clontech). pGBKT7-Irgm1 served as bait to screen a hightiter murine embryonic fibroblast (MEF) library expressed in pACT2. pGBKT7-Irgm1 plus the pACT2 library were introduced into *Saccharomyces cerevisiae* AH109, and bacteria were successively plated for 7 days at 30°C on SD medium lacking histidine, leucine, and tryptophan (SD-HLT) and SD medium lacking adenine, histidine, leucine, and tryptophan (SD-AHLT) in the presence of X-αGal (5-bromo-4-chloro-3-indolyl-αD-galactopyranoside) Positive phenotype (“blue”) colonies were isolated, and pACT2 cDNA inserts in these colonies were rescued and confirmed via retransformation. Isolates were then subjected to a third-round stringency screen, after which DNA prepared, sequenced and analyzed by BLAST search. pGBKT7-cI + pACT2-cI containing the bacteriophage lambda cI gene fragment that encodes a repressor protein homodimeric domain served as a positive control.

Co-immunoprecipitation and GST pulldown assays

For co-IP assays, HEK cells expressing either Flag- or Myc-tagged proteins along with the respective EGFP-tagged partner proteins were lysed in RIPA buffer (150mM NaCl, 1% NP-40,0.5% DOC, 0.1% SDS, 50mM Tris pH 8.0, protease inhibitors and phosphatase inhibitors for PI(3)K) and clarified by centrifugation at 4°C. Whole cell lysates (WCL) were pre-cleared with protein A/G Sepharose beads to eliminate nonspecific binding and supernatants were incubated with the respective antibodies; immunoprecipitates were then washed and subjected to immunblot. GST pulldown assays consisted of soluble rGST or rGST-tagged proteins immobilized on glutathione-Sepharose 4B beads that were incubated with pre-cleared WCL containing transiently-expressed Flag-Pik3ca and Pik3r1-Flag. Beads were extensively washed and immunoblotted as described above.

Statistics

Differences between control and experimental groups were analyzed via single factor analysis of variance (ANOVA) or Student's t-test. *P* values less than the threshold statistic is shown.

Supplementary Material

Refer to Web version on PubMed Central for supplementary material.

ACKNOWLEDGEMENTS

We thank L. Cantley (Harvard Medical School), P. De Camilli, J. Galan, P. Lengyel, R. Lin (Stony Brook University), J. Lucocq (University of Dundee), T. Meyer (Stanford University), C. Roy, B. Vanhaesebroeck (University of London), and G. Warren (Vienna Biocenter) for antibodies, plasmids or cDNAs used in this study, P. Cresswell for the Y2H MEF library, G. Taylor (Duke University Medical Center) for *Irgm1*$^{-/-}$ mice, Y. Lu (University of Iowa) for BCG-GFP and A. Shenoy for Irgm1 crystallographic modeling. Support was provided by NIH NIAD R01 (AI068041-01A1), Burroughs-Wellcome Fund Investigator in Infectious Disease Award (1007845), Edward R. Mallinckrodt Foundation (R06152), Searle Foundation Scholars Program (05-F-114), Cancer Research Institute Investigator Award Program, W.W. Winchester Foundation (to J.D.M.) and Japanese Society for the Promotion of Science (to T.M.).

References

1. Hingley-Wilson SM, Sambandamurthy VK, Jacobs WR Jr. Survival perspectives from the world's most successful pathogen, *Mycobacterium tuberculosis*. Nat. Immunol. 2003; 4:949–955. [PubMed: 14515128]
2. Pieters J. *Mycobacterium tuberculosis* and the macrophage. Maintaining a balance. Cell Host & Microbe. 2008; 3:399–407. [PubMed: 18541216]
3. MacMicking JD, Taylor GA, McKinney JD. Immune control of tuberculosis by IFN-γ-inducible LRG-47. Science. 2003; 302:654–659. [PubMed: 14576437]
4. Gutierrez MG, et al. Autophagy is a defense mechanism inhibiting BCG and *Mycobacterium tuberculosis* survival in infected macrophages. Cell. 2004; 119:753–766. [PubMed: 15607973]
5. Singh SB, Davis AS, Taylor GA, Deretic V. Human IRGM induces autophagy to eliminate intracellular bacteria. Science. 2006; 313:1438–1441. [PubMed: 16888103]
6. Xu Y, et al. Toll-like receptor 4 is a sensor for autophagy associated with innate immunity. Immunity. 2007; 27:135–144. [PubMed: 17658277]
7. Feng CG, et al. Mice deficient in LRG-47 display increased susceptibility to mycobacterial infection associated with the induction of lymphopenia. J. Immunol. 2004; 172:1163–1168. [PubMed: 14707092]
8. MacMicking JD, et al. Identification of nitric oxide synthase as a protective locus against tuberculosis. Proc. Natl Acad. Sci. USA. 1997; 94:5243–5248. [PubMed: 9144222]
9. Ng VH, Cox JS, Sousa AO, MacMicking JD, McKinney JD. Role of *KatG* catalase-peroxidase in mycobacterial pathogenesis: Countering the oxidative burst. Mol. Microbiol. 2004; 52:1291–1302. [PubMed: 15165233]
10. Malik S, et al. Alleles of the *NRAMP1* gene are risk factors for pediatric tuberculosis disease. Proc. Natl Acad. Sci. USA. 2005; 102:12183–12188. [PubMed: 16103355]
11. Bekpen C, et al. The interferon-inducible p47 (IRG) GTPases in vertebrates: loss of the cell autonomous resistance mechanism in the human lineage. Genome. Biol. 2005; 6:R92. [PubMed: 16277747]
12. Shenoy AR, et al. Emerging themes in IFN-γ-induced macrophage immunity by the p47 and p65 GTPase families. Immunobiology. 2008; 8:771–784.
13. Taylor GA, Feng CG, Sher A. p47 GTPases: regulators of immunity to intracellular pathogens. Nat. Rev. Immunol. 2004; 4:100–109. [PubMed: 15040583]

14. MacMicking JD. IFN-inducible GTPases and immunity to intracellular pathogens. Trends Immunol. 2004; 25:601–609. [PubMed: 15489189]
15. Stephens DJ, Banting G. Specificity of interaction between adaptor-complex medium chains and the tyrosine-based sorting motifs of TGN38 and lgp120. Biochem. J. 1998; 335:567–572. [PubMed: 9794796]
16. Martens S, et al. Mechanisms regulating the positioning of mouse p47 resistance GTPases LRG-47 and IIGP1 on cellular membranes: retargeting to plasma membrane induced by phagocytosis. J. Immunol. 2004; 173:2594–2606. [PubMed: 15294976]
17. Ghosh A, Uthaiah R, Howard J, Herrmann C, Wolf E. Crystal structure of IIGP1: a paradigm for interferon-inducible p47 resistance GTPases. Mol. Cell. 2004; 10:727–739. [PubMed: 15350217]
18. McLaughlin S, Murray D. Plasma membrane phosphoinositide organization by protein electrostatics. Nature. 2005; 438:605–611. [PubMed: 16319880]
19. Manna D, Albanese A, Park WS, Cho W. Mechanistic basis of differential cellular responses of phosphatidylinositol 3,4-bisphosphate- and phosphatidylinositol 3,4,5-trisphosphate-binding pleckstrin homology domains. J. Biol. Chem. 2007; 282:32093–32105. [PubMed: 17823121]
20. Chua J, Deretic V. *Mycobacterium tuberculosis* reprograms waves of phosphatidylinositol 3-phosphate on phagosomal organelles. J. Biol. Chem. 2004; 279:36983–36992.
21. Fischer K, et al. Mycobacterial lysocardiolipin is exported from phagosomes upon cleavage of cardiolipin by a macrophage-derived lysosomal phospholipase A2. J Immunol. 2001; 167:2187–92. [PubMed: 11490004]
22. Koyasu S. The role of PI(3)K in immune cells. Nat. Immunol. 2003; 4:313–319. [PubMed: 12660731]
23. Kamen LA, Levinsohn J, Swanson JA. Differential association of phosphatidylinositol 3-kinase, SHIP-1, and PTEN with forming phagosomes. Mol. Biol. Cell. 2007; 18:2463–2472. [PubMed: 17442886]
24. Kamen LA, Levinsohn J, Cadwallader A, Tridandapani S, Swanson JA. SHIP-1 increases early oxidative burst and regulates phagosome maturation in macrophages. J. Immunol. 2008; 180:7497–7505. [PubMed: 18490750]
25. Heo WD, et al. PI(3,4,5)P_3 and PI(4,5)P_2 lipids target proteins with polybasic clusters to the plasma membrane. Science. 2006; 314:1458–1461. [PubMed: 17095657]
26. Vieira O, et al. Distinct roles of class I and class III phosphatidylinositol 3-kinases in phagosome formation and maturation. J. Cell Biol. 2001; 155:19–25. [PubMed: 11581283]
27. Vanhaesebroeck B, et al. Synthesis and function of 3-phosphorylated inositol lipids. Ann. Rev. Biochem. 2001; 70:535–602. [PubMed: 11395417]
28. Hayakawa M, et al. Synthesis and biological evaluation of 4-morpholino-2-phenylquinazolines and related derivatives as novel PI3 kinase p110alpha inhibitors. Bioorg. Med. Chem. 2006; 14:6847–6858. [PubMed: 16837202]
29. Jackson SP, et al. PI3-kinase p110beta: a new target for antithrombotic therapy. Nat. Med. 2005; 11:507–514. [PubMed: 15834429]
30. Condliffe AM, et al. Sequential activation of class IB and class 1A PI(3)K is important for the primed respiratory burst of human but not murine neutrophils. Blood. 2005; 106:1432–1440. [PubMed: 15878979]
31. Rodriguez-Viciana P, et al. Phosphatidylinositol-3-OH kinase as a direct target of Ras. Nature. 1994; 370:527–532. [PubMed: 8052307]
32. Chamberlain MD, Berry TR, Pastor MC, Anderson DH. The p85alpha subunit of phosphatidylinositol 3'-kinase binds to and stimulates the GTPase activity of Rab proteins. J. Biol. Chem. 2004; 279:48607–48614. [PubMed: 15377662]
33. Bos JL, Rehmann H, Wittinghofer A. GEFs and GAPs: critical elements in the control of small G proteins. Cell. 2007; 129:865–877. [PubMed: 17540168]
34. Buxton P, Zhang XM, Walsh B, Sriratana A, Schenberg I, Manickam E, Rowe T. Identification and characterization of Snapin as a ubiquitously expressed SNARE-binding protein that interacts with SNAP23 in non-neuronal cells. Biochem. J. 2003; 15:433–440. [PubMed: 12877659]
35. Pan PY, Tian JH, Sheng ZH. Snapin facilitates the synchronization of synaptic vesicle fusion. Neuron. 2009; 61:412–424. [PubMed: 19217378]

36. Lu L, Cai Q, Tian JH, Sheng ZH. Snapin associates with late endocytic compartments and interacts with late endosomal SNAREs. Biosci. Rep. Apr 1.2009 [Epub ahead of print].
37. Stamnes MA, Craighead MW, Hoe MH, Lampen N, Geromanos S, Tempst P, Rothman JE. An integral membrane component of coatomer-coated transport vesicles defines a family of proteins involved in budding. Proc. Natl. Acad. Sci. USA. 1995; 92:8011–8015. [PubMed: 7644530]
38. Hawkins PT, Anderson KE, Davidson K, Stephens LR. Signaling through class I PI(3)Ks in mammalian cells. Biochem. Soc. Trans. 2006; 34:647–662. [PubMed: 17052169]
39. Deb DK, et al. Activation of protein kinase C delta by IFN-γ. J. Immunol. 2003; 171:267–273. [PubMed: 12817007]
40. Yeung T, et al. Receptor activation alters inner surface potential during phagocytosis. Science. 2006; 313:34–351. [PubMed: 16825547]
41. Ferguson KM, et al. Structural basis for the discrimination of 3-phosphoinositides by pleckstrin homology domains. Mol. Cell. 2000; 6:373–384. [PubMed: 10983984]
42. Rodriguez-Viciana P, et al. Role of phosphoinositide 3-OH kinase in cell transformation and control of actin cytoskeleton by Ras. Cell. 1997; 89:457–467. [PubMed: 9150145]
43. Christoforidis S, et al. Phosphatidylinositol-3-OH kinases are Rab5 effectors. Nat. Cell Biol. 1999; 1:249–252. [PubMed: 10559924]
44. Zhao Z, et al. Autophagosome-independent essential function for the autophagy protein Atg5 in cellular immunity to intracellular pathogens. Cell Host Microbe. 2008; 4:458–69. [PubMed: 18996346]
45. Jayachandran R, et al. Survival of mycobacteria in macrophages is mediated by coronin 1-dependent activation of calcineurin. Cell. 2007; 130:37–50. [PubMed: 17632055]
46. Kuijl C, et al. Intracellular bacterial growth is controlled by a kinase network around PKB/AKT1. Nature. 2007; 450:725–730. [PubMed: 18046412]
47. Feng CG, et al. The immunity-related GTPase Irgm1 promotes the expansion of activated $CD4^+$ T cell populations by preventing interferon-γ-induced cell death. Nat. Immunol. 2008; 9:1279–1287. [PubMed: 18806793]
48. Luo Y, Szilvasi A, Chen X, DeWolf WC, O'Donnell MA. A novel method for monitoring *Mycobacterium bovis* BCG trafficking with recombinant BCG expressing green fluorescent protein. Clin. Diagn. Lab Immunol. 1996; 3:761–768. [PubMed: 8914772]
49. Taguchi T, Pypaert M, Warren G. Biochemical sub-fractionation of the mammalian Golgi apparatus. Traffic. 2003; 4:344–352. [PubMed: 12713662]
50. Mileykovskaya E, et al. Cardiolipin binds nonyl acridine orange by aggregating the dye at exposed hydrophobic domains on bilayer surfaces. FEBS Lett. 2001; 507:187–190. [PubMed: 11684095]

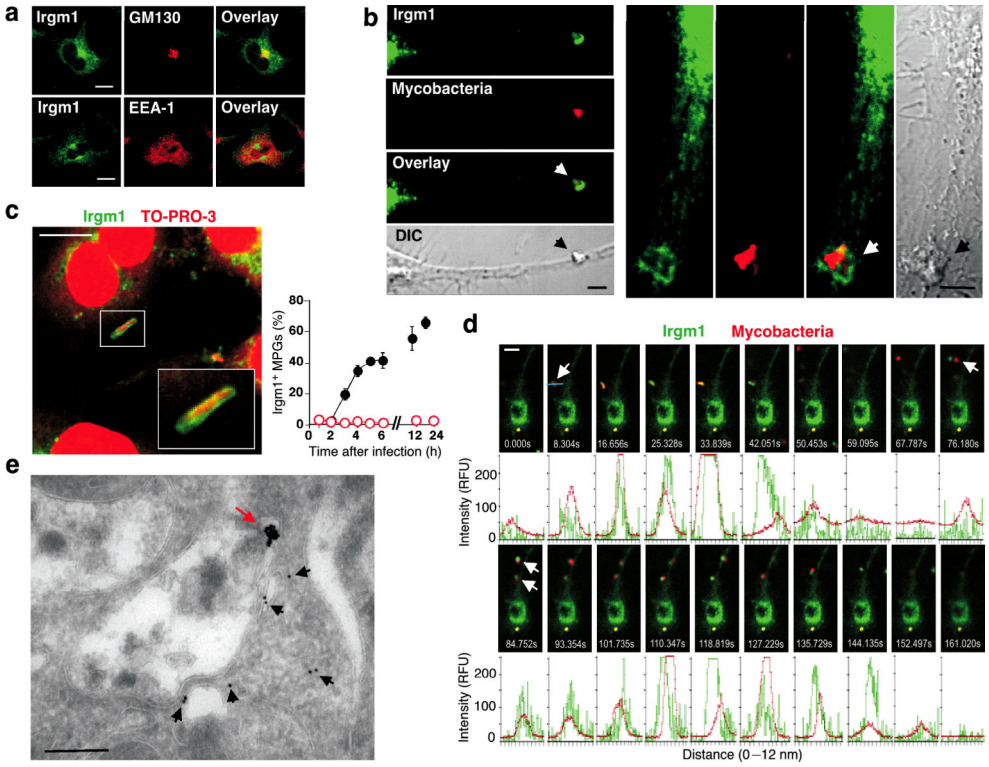

Figure 1.

Endogenous Irgm1 traffics from the *cis*-Golgi to MPGs in IFN-γ-activated macrophages. (**a**) IFN-γ-activated (24h, 100U/ml) RAW264.7 cells were stained with Alexa488-conjugated anti-Irgm1 plus Alexa594-conjugated anti-GM130 mAb (top) or Alexa594-conjugated anti-EEA-1 (bottom). Scale bar, 10μm. (**b**) BMMs (left) or RAW264.7 cells (right) were chased for 30 min with *M. bovis* BCG Phipps (MOI 2: 1), after which cells were stained with Alexa488-conjugated anti-Irgm1 and Alexa594-conjugated anti-*Mtb* complex to detect nascent MPGs. Arrowheads, MPGs; scale bar, 2μm; DIC, Differential Interference Contrast. Images selected from 3-4 independent experiments. (**c**) Left, RAW264.7 cells stained at 6 h p.i. with TO-PRO-3 to detect bacterial and host nuclear DNA and anti-Irgm1. Inset, Irgm1-"coated" MPG. Right, Percent of total MPGs that were Irgm1$^+$ in IFN-γ-treated (filled circles) or untreated (open circles) macrophages at various times p.i. (>300 MPGs counted/time point). (**d**) IFN-γ-activated RAW264.7 cells expressing RFP-Irgm1 (pseudocolored green) were infected with EGFP-expressing *M. bovis* BCG Pasteur (pseudocolored red) and subjected to live imaging. Blue bar placed across the lower mycobacterium (depicted here in the first frame only) yielded fluorescence intensity plots for Irgm1 and *M. bovis* below. White arrows depict both lower and upper bacteria. Scale bar, 5μm. Representative of 8 movies collected. (**e**) EM of immuno-labeled cryosections showing 15nm BSA-gold fused *M. bovis* BCG phagolysosomes (red arrow) harboring endogenous Irgm1 (10nm Protein A-gold; black arrows) in IFN-γ-activated RAW264.7 cells at 6 h p.i. BSA-gold was pulse-chased into lysosomes overnight. Scale bar, 400nm.

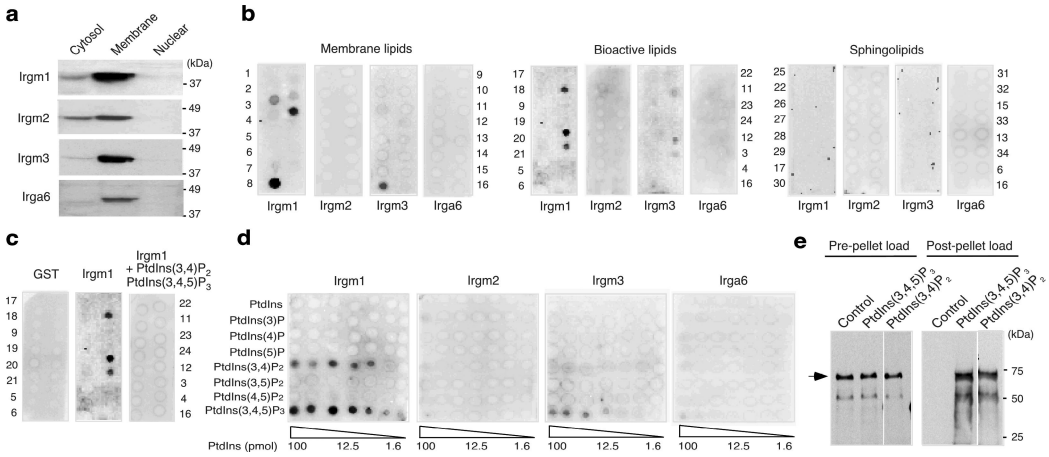

Figure 2.

Irgm1 is a membrane-associated protein that binds PtsIns(3,4,5)P_3**,** PtdIns(3,4)P_2, and diphosphatidylglycerol **(a)** IFN-γ-activated macrophage sub-fractions were immunoblotted with Irgm1 or $_p$47 GTPase-specific antibodies. Irgm1 migrates slightly below its predicted M_r. One of three sub-fractionation experiments shown. (**b**) Protein gel overlay using 5μg/ml rGST-Irgm1, rGST-Irgm2, rGST-Irgm3 or rGST-Irgb6. 1, triglyceride; 2, diacylglycerol; 3, phosphatidic acid; 4, phosphatidylserine; 5, phosphatidylethanolamine; 6, phosphatidylcholine; 7, phosphatidylglycerol; 8, diphosphatidylglycerol; 9, phosphatidylinositol (PtdIns); 10, PtdIns(4)P; 11, PtdIns(3,4)P_2; 12, PtdIns(3,4,5)P_3; 13 cholesterol; 14, sphingomyelin; 15, sulfatide; 16, Solvent blank; 17, lysophoshatidic acid; 18, lysophosphocholine; 19, PI(3)P; 20, PtdIns(4)P; 21, PtdIns(5)P; 22, sphingosine-1-phosphate; 23, PtdIns(3,5)P_2; 24, PtdIns(4,5)P_2; 25, sphingosine; 26, phytosphingosine; 27, ceramide; 28, sphingomyelin; 29, sphingosylphosphatidylcholine; 30, myriocin; 31, monosialoganglioside G_{M1}; 32, disialoganglioside; 33, sphingosylgalactoside; 34, lysophosphatidylcholine. (**c**) Protein gel overlay using rGST alone, rGST-Irgm1 or rGST-Irgm1 pre-incubated with 15-fold molar excess of PtdIns(3,4)P_2 and PtdIns(3,4,5)P_3. rGST-Irgm1 bioactive lipids strip from (**b**) included for comparison. (**d**) Dose-responsive lipid binding to rGST fusion proteins. One of three gel overlay experiments shown. (**e**) rGST-Irgm1 was incubated with liposomes containing 5% mol/mol PtdIns(3,4)P_2 or PtdIns(3,4,5)P_3. Material was analyzed by immunoblot with anti-GST prior to (pre-pellet) and after (post-pellet) sedimentation by centrifugation. One of four sedimentation assays shown.

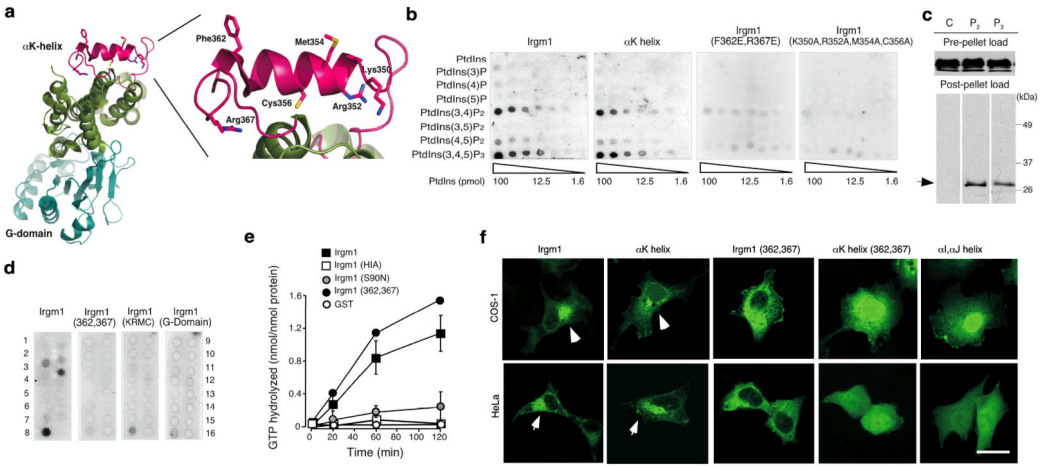

Figure 3.

An Irgm1 C-terminal amphipathic helix confers membrane binding *in vitro* and *in vivo*. (**a**) Irgm1 structure based on dimeric Irgb6 (PDB code 1TQ2:2) depicting the membrane-accessible αK helix. Inset. Mutations generated within this region. (**b**) PtdIn binding profile for matched molar equivalents of rGST-Irgm1 (5μg/ml), rGSTμK (1.9μg/ml), rGSTIrgm1(F362E,R367E) (5μg/ml) and rGST-Irgm1(K350,R352,M354A,C356) (5μg/ml) in gel overlay. Derived from 2-3 independent overlay assays. (**c**) rGST-αK was incubated with liposomes containing no PtdIns (Control, C) or liposomes containing 5% w/w PtdIns(3,4)P_2 (P_2) or PtdIns(3,4,5)P_3 (P_3). Material was analyzed by immunoblot with anti-GST prior to (pre-pellet) or after (post-pellet) sedimentation by centrifugation. One of two sedimentation assays shown. (**d**) Lipid-binding profile of rGST-Irgm1(F362E,R367E) (labeled 362,367) (5μg/ml), rGSTIrgm1(K350,R352,M354A,C356) (labeled KMRC) (5μg/ml) and catalytically-active G-domain fragment (rGST-GD75-292; 3.8μg/ml). The membrane lipids strip from Fig. 2(b) included for comparison. (**e**) Intrinsic GTPase activity of lipid-binding and non-binding Irgm1 variants in $\tilde{\gamma}[^{32}P]$GTP hydrolysis assays. GST, heat-inactivated (HIA) GST-Irgm1 and catalytically-inactive rGST-Irgm1(S90N) were negative controls. Mean ± SD of triplicate samples. One of 4 independent assays shown. (**f**) COS1 or HeLa cells were nucleoporated with N-terminal EGFP-tagged Irgm1 variants. White arrows indicate Golgi membrane targeting. Scale bar, 10μm Images collected from ~150 transfected cells examined per plasmid in 2 separate experiments.

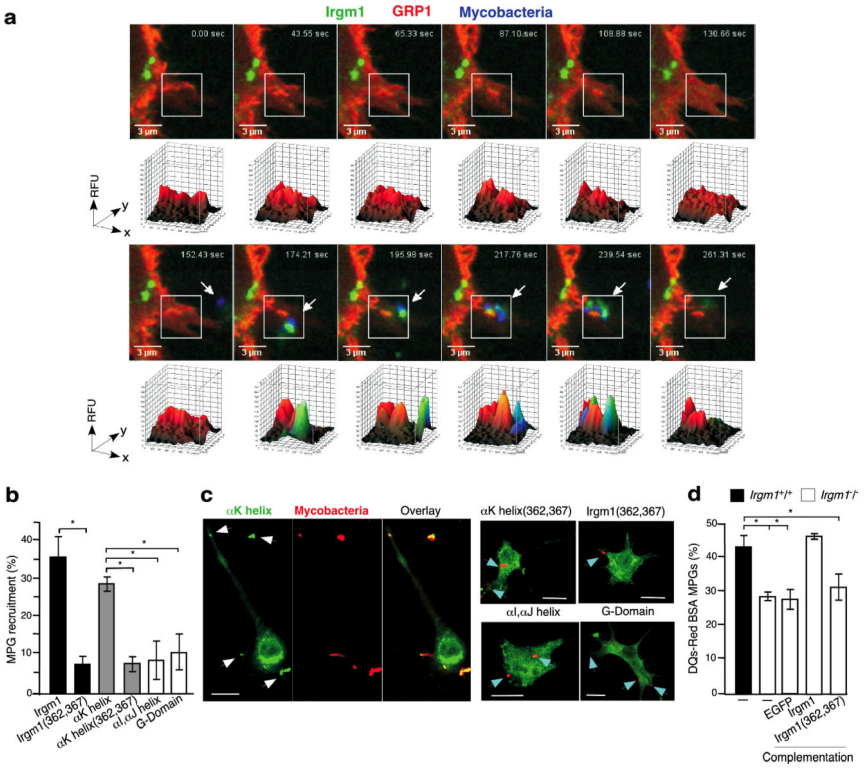

Figure 4.

Irgm1 recruitment to PtdIns-enriched membranes for phagolysosomal fusion requires its αK helix. (**a**) Triple-labeled live imaging of Irgm1 translocation to PtdIns(3,4,5)P_3-pseudopods internalizing BCG in IFN-γ-activated RAW264.7 cells. CFP-Irgm1 (pseudocolored green); YFP-GRP1-PH (pseudocolored red); Cy5-BCG. 3D surface intensity plots (white boxes) below each frame. (**b**) Percent of MPGs targeted by EGFP-αK, EGFP-αK(F362E,R367E) (labeled 362,367), EGFP-Irgm1(F362E,R367E) (labeled 362,367), EGFP-αI,αJ or EGFP-GD_{75}-292 (labeled G-domain) within IFN-γ-activated macrophages (60 min pulse, 3h p.i.). 250-440 MPGs were counted per Irgm1 variant from 3 transfection experiments. *, $P <$ 0.012 (Student's t-test). (**c**) MPG targeting of Irgm1 variants in IFN-γ-activated RAW264.7 macrophages. White and blue arrows depict targeted and non-targeted PGs, respectively. Scale bar, 10μm. (**d**) Complementation of MPG-lysosome fusion (DQ-Red BSA dequenching) in IFN-γ-activated primary *Irgm1*$^{-/-}$ BMMs (24 h p.i.) by EGFP-Irgm1 but not EGFP or EGFP-Irgm1(362,367). More than 600 MPGs were counted for each transfection in 2 experiments. *, $P < 0.029$ (single factor analysis of variance, ANOVA).

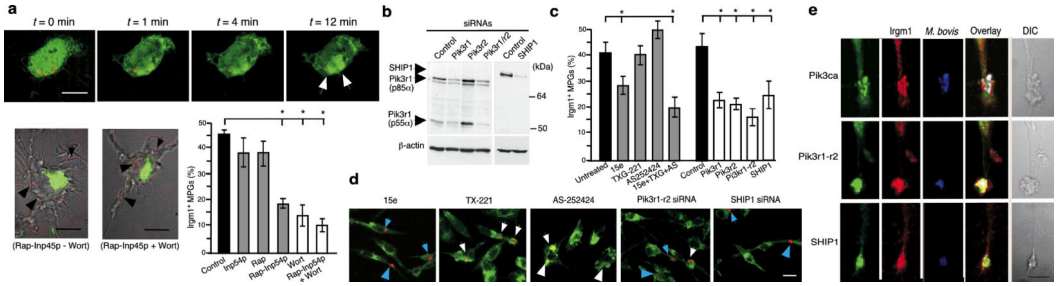

Figure 5.

Pik3ca-Pik3r1-r2 heterodimers furnish PtdIns(3,4,5)P_3 and PtdIns(3,4)P_2 on MPGs for Irgm1 recruitment. **(a)** PtdIns(3,4,5)P_3 **w**as depleted from MPGs in IFN-γ-activated RAW264.7 cells using rapamycin (Rap)-induced dimerization of an FBP-tagged Inp54p phosphatase, which is targeted to PGs (white arrows) via its interactions with a FKBP-tagged Lyn motif. CFPInp54p-FRB (pseudocolored green). Cy5-BCG (pseudocolored red). Time after Rap treatment shown above. Top, representative movie. Scale bar, 5μm. Bottom left, DIC overlay of In54p-expressing IFN-γ-activated macrophages treated or not with wortmanin (Wort) to remove residual PtdIns(3,4,5)P_3. YFP-Irgm1 (green), Cy5-BCG (pseudocolored red; 30 min chase). CFP channel was turned off to reveal loss of Irgm1 translocation. Bottom right, Percent of MPGs containing Irgm1 in cells treated as indicated. 150-220 MPGs were counted per treatment in 3 separate experiments. *, $P < 0.0002$ (ANOVA). (**b**) Efficiency of siRNA silencing in IFN-γ-activated RAW264.7 macrophages. Indicated PI(3)Kr isoforms and SHIP1 were detected by immunoblot. γ-actin, loading control. (**c**) Effect of Class I PI(3)K isoform-specific inhibition via chemical compounds (left) or siRNA (right) on Irgm1 recruitment to MPGs. 280-320 MPGs were counted in 4 separate experiments. *, $P < 0.0025$ (ANOVA). (**d**). Lower magnification of siRNA- or chemically-treated IFN-γ-activated macrophages. Cells fixed in 3% PFA were stained with Alexa488-conjugated anti-Irgm1 and Alexa488-conjugated anti-*Mtb* complex. White arrows, Irgm1-containing MPGs; Blue arrows, MPGs lacking Irgm1. Scale bar, 10μm. (**e**) Triple-color plus DIC sCFM overlay showing endogenous PI(3)K subunits or SHIP1 with Irgm1 on phagocytic cups engulfing Cy5-*M. bovis* BCG. Scale bar, 2μm.

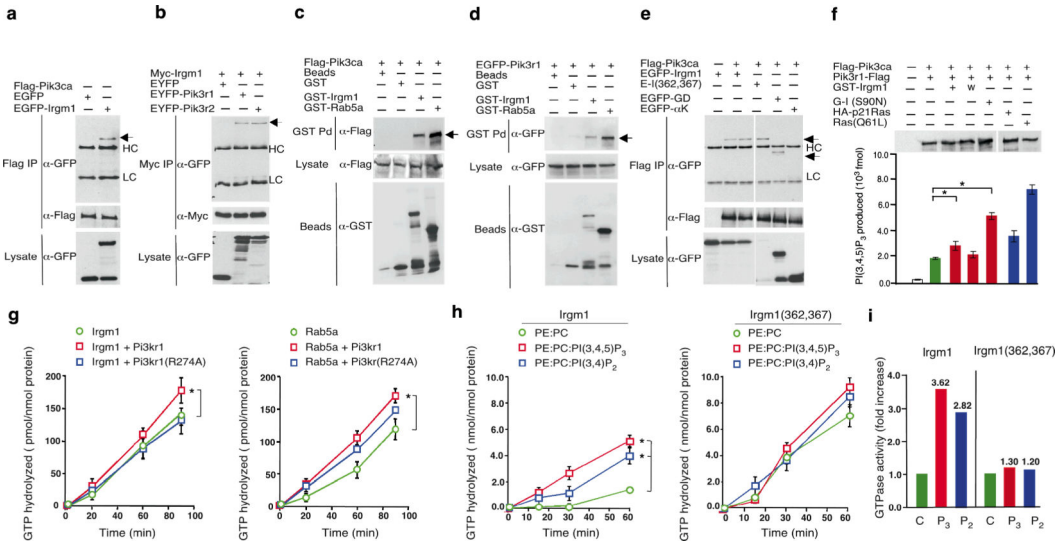

Figure 6.

Spatial Irgm1 and PI(3)K convergence confers direct cross-regulatory functions. (**a,b**) HEK cells transfected with indicated Flag-tagged or Myc-tagged constructs were subject to immunoprecipitation and immunoblot. Arrows indicate bound partner. HC, IgG_1 heavy chain, LC, IgG_1 light chain. One of 3 experiments shown. (**c,d**) GST pulldown (Pd) of Flag-Pik3ca or EGFP-Pik3r1 expressed in HEK cells by GST-Irgm1 or a positive control, GST-Rab5a (black arrows). GST protein captured on Sepharose 4B beads is shown. First lane, beads alone. One of 2 experiments shown (**e**) Binding of wild-type and mutant Irgm1 to Pik3ca in HEK cell lysates was determined as in panel a. E-I (362,367), EGFP-Irgm1(362,367). (**f**) Lipid kinase activityof Flag-Pik3ca-Flag-Pi in the presence or absence of Irgm1. Positive controls, HA-tagged $p21^{Ras}$ GTPase or HA-tagged $p21^{RasQ61L}$. Top, immunoblot of rate-limiting catalytic 110kDa Pik3ca subunit captured on Protein G-agarose. Bottom, mean ± SD of triplicate samples. One of 3 assays shown. *, $P < 0.027$ (ANOVA). G-1(S90N), GST-Irgm1(S90N). (**g**) Single turnover γ-[^{32}P]GTP hydrolysis by rGST-Irgm1 bound to rPik3r1 or rPik3r1(R274A). rGST-Rab5a (positive control). Mean ± SD of triplicate samples. Data are from two independent assays. *, $P < 0.048$ (Students t-test). (**h**) Continuous $\tilde{\gamma}$-[^{32}P]GTP hydrolysis by rGST-Irgm1 or rGST-Irgm1(F362E,R367E) bound to 100nm PE:PC liposomes containing PtdIns(3,4,5)P_3 or PtdIns(3,4)P_2. Mean ± SD of triplicate samples from two independent assays. *, $P < 0.014$ (ANOVA). PC:PE control liposomes not containing PtdIns. (**i**) Fold-change in GTPase activity of Irgm1 proteins bound to PtdIns(3,4,5)P_3 (P_3)-containing or PtdIns(3,4)P_2 (P_2)-containing lipid bilayers, versus Irgm1 proteins bound to control (C) PtdIns-deficient bilayers.

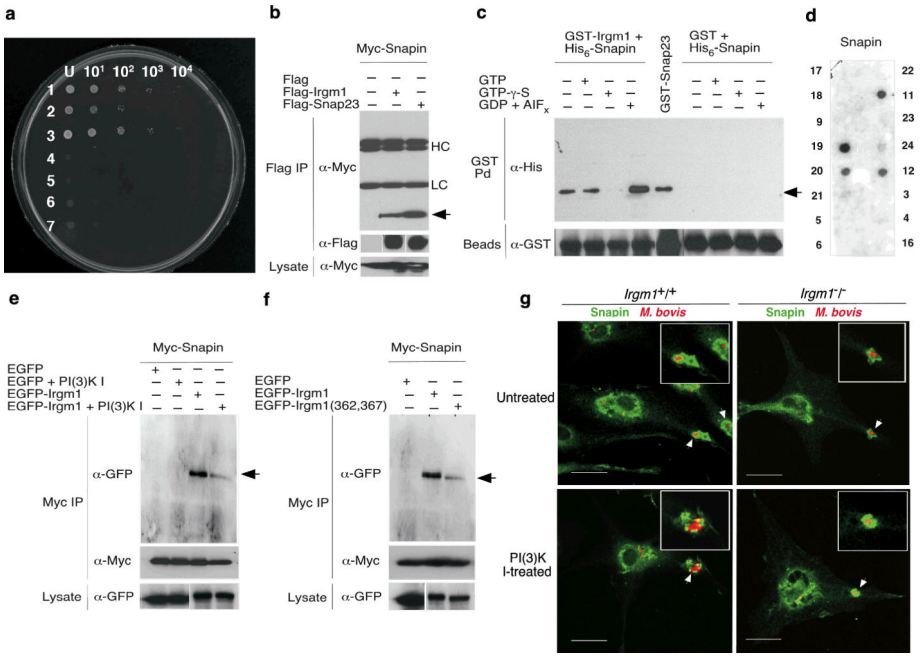

Figure 7.

PtdIns(3,4,5)P_3 and PtdIns(3,4)P_2 production promotes Irgm1 effector binding at MPGs.(**a**) The t-SNARE adaptor snapin as an interacting partner of Irgm1. Yeast AH109 co-transformation (72 h; horizontal dilutions) in 2-hybrid analysis on SD-AHLT plates. 1, pGBKT7-cI + pACT2-cI (positive control); 2, pGBKT7-Irgm1 + pACT2-Snapin; 3, pGBKT7-Irgm1 + pACT2-Tmed10; 4, pGBKT7-Irgm1 + pACT2-cI; 5, pGBKT7-Irgm1 + pACT2; 6, pGBKT7-cI + pACT2-Snapin; 7, pGBKT7-cI + pACT2-Tmed10. Conditions 4-7 served as individual negative controls. U, undiluted. (**b**) Co-immunoprecipitation of Myc-Snapin by Flag-Irgm1 in HEK cells. Arrow depicts Snapin. HC, heavy chain; LC, light chain. Flag-Snap23 (positive control). One of 4 independent experiments shown. (**c**) Conformation-dependent association of GST-Irgm1 with His_6-Snapin in the free, GTP (1mM), GTP-γ-S (1mM) or GDP (0.1μM) + AIF_x (100μM $AlCl_3$/15mM NaF)-bound state. Compounds were added 60 min at 4°C prior to incubation of GST-Irgm1 with His_6-Snapin. GST, negative control. GST proteins bound to Snapin (1:6 stoichiometry, Supplementary Fig. 9 online) were immunoblotted with anti-His_6-Snapin One of 3 pulldown experiments shown. (**d**) Protein gel overlay of untagged Snapin (5μg/ml) detected by anti-Snapin. Lipid numbers match those in **Fig. 2b**. (**e,f**) Impaired binding of Snapin to Irgm1 in HEK cells treated with class I PI(3)K inhibitors (I; 15e + TXG-221 + 252424) or expressing EGFP-Irgm1(362,367). (**g**) Primary IFN-γ-activated wild-type and *Irgm1-/-* macrophages were treated or not treated with class I PI(3)K inhibitors, and were infected with Cy5-labeled *M. bovis*. Three hours after infection cells were stained with anti-Snapin. Arrows, PGs. Scale bar, 10μm.